Thiol-assisted aerosol synthesis of mesoporous Cu-SiO_2 catalysts for effective and stable ethanol dehydrogenation

Giovanni Pampararo[1]*, Marc Antoine Colinet[1], Francois Devred[1], Damien P. Debecker[1]*

* Giovanni.Pampararo@uclouvain.be, Damien.Debecker@uclouvain.be

1. Université catholique de Louvain (UCLouvain), Institute of Condensed Matter and Nanosciences (IMCN), Place Louis Pasteur 1, Louvain-la-Neuve, 1348, Belgium

Abstract: Supported copper nanoparticles play a fundamental role in heterogeneous sustainable catalysis, particularly for the conversion of biomass-derived feedstocks (such as bioethanol) to platform chemicals. However, controlling their fine dispersion and, at the same time, their resistance to sintering remains a challenge, especially when using silica supports. We report a simple one-pot aerosol route to produce mesoporous Cu–SiO_2 catalysts featuring small copper nanoparticles (2~4 nm) partially embedded in the silica matrix. To achieve this, we exploit the affinity between the copper and the thiol function of a mercapto-silane: (3-mercaptopropyl)-trimethoxysilane (MPTMS). As supported by characterization (in particular XRD, XPS, TEM, TPR, Uv-VIS, and dispersion measurements) the addition of this molecule during synthesis markedly enhanced Cu dispersion in the calcined catalyst. This is shown to translate into enhanced time-on-stream stability during the ethanol non oxidative dehydrogenation to acetaldehyde. The catalyst obtained via thiol-assisted stabilization of copper demonstrates a sustained acetaldehyde productivity of 2.88 $g_{aca}*g_{cat}^{-1}*h^{-1}$ during 23 h test time at 623 K.

Keywords: Cu-based catalysts, bioethanol, HSAB theory, MPTMS, EISA process, dehydrogenation, stability, deactivation.

1. INTRODUCTION

Bioethanol is a versatile renewable platform chemical for sustainable catalysis, enabling the synthesis of a wide range of commodity chemicals such as ethyl acetate[1], butanol[2], ethylene[3–5], acetaldehyde[6], and green hydrogen.[6,7] In this context, copper-based catalysts have shown considerable promise [8,9] because of their capacity to selectively promote α-C–H bond activation of adsorbed ethoxy species (the rate-limiting step), resulting in acetaldehyde and molecular hydrogen formation.[6,10,11] However, their widespread implementation is hindered by on-stream deactivation phenomena, mainly related to metal sintering and carbonaceous materials deposition.[12–14] We have previously reported the preparation of copper–silica catalysts via the aerosol-assisted sol–gel (AASG) method[15], which exhibited superior catalytic performance compared to benchmark materials synthesized by conventional impregnation techniques.[16] The method consists in leveraging a rapid sol-gel process to incorporate a Cu salt into a mesoporous silica material, and applying a controlled calcination to trigger the exsolution of CuO nanoparticles. These are then available on the surface for catalysis and remain well anchored to the silica matrix. Nevertheless, during extended catalytic testing, deactivation still occurred, primarily due to the tendency of the smallest metallic copper nanoparticles to agglomerate. Although this phenomenon was significantly mitigated compared to impregnated catalysts, it highlighted the persisting challenge of mitigating sintering.

A further strategy to stabilize Cu species within the support matrix can be derived from the Hard and Soft Acids and Bases (HSAB) theory. [17] According to this concept, incorporating elements that exhibit a strong affinity for Cu^{2+} - particularly soft or borderline bases such as sulfur or nitrogen - during the synthesis can enhance metal–support interactions. In the case of silica, while the hard acid Si^{4+} preferentially coordinates with hard bases like O^{2-} to form the SiO_2 pattern, introduced heteroatoms such as SH can act as softer electron donors capable of interacting more strongly with Cu^{2+} or Cu^{+} species.[18,19] For example, to increase the affinity between the silica surface and gold, silica has been already modified with organic linkers.[20,21] In this light, the introduction of soft ligands such as sulfur-containing moieties (e.g., thiols) has garnered increasing interest also for catalysis.[22–24] Recent studies have demonstrated that incorporating thiol-functionalized silanes - such as (3-mercaptopropyl)trimethoxysilane (MPTMS) - during catalyst synthesis can substantially enhance metal dispersion and thermal stability, as evidenced in the case of gold. [25]

Regarding Cu and MTPMS, except cases where the functionalization aimed at metal adsorption for environmental purpose,[26] few are the example in literature for catalysis. Galehban et al. [27]

reported stable and reusable Fe_3O_4@SiO_2@KCC-1@MPTMS@Cu II mesoporous nanocomposite for the reduction of nitroarenes and coumarin synthesis in batch liquid reactor. Zhan et al. [28] observed that Cu_2O nanoparticles become structurally integrated into the silica matrix through Cu–S interactions (via MPTMS). Such Cu–organosilica materials were successfully employed for the reduction of 4-nitrophenol. Sulfur-based coordination, while useful for structuring hybrid materials, limits their application under high-temperature catalytic conditions due to thermal instability and ligand decomposition—conditions critical for industrial relevance.

In this work, we introduce a novel strategy that transiently employs sulfur to coordinate copper during the AASG process (see Scheme S1), stabilizing highly dispersed Cu species within a silica matrix. The sulfur-based promoter is then removed during calcination, yielding a thermally robust material suitable for demanding catalytic applications. We investigate the effect of MPTMS on the textural, structural, and catalytic properties of the obtained copper–silica catalysts. Emphasis is placed on understanding the role of thiol functionalities in modulating copper dispersion and sintering resistance, during bioethanol dehydrogenation reaction.

2. EXPERIMENTAL SECTION

2.1 Catalysts preparation

Solution A was prepared by mixing TEOS (TCI Chemicals, >97%) with 20g of an aqueous HCl solution (pH=2), which was achieved by diluting fuming HCl (Roth, 37 wt.%). In this solution, a certain amount of with (3-Mercaptopropyl)trimethoxysilane (TCI Chemicals, >96%) was added as well (see below). Solution B consisted of 45g of ethanol (VWR, >99.8% v/v), 8 g of distilled water, and 3.88 g of Pluronic® F127 (Sigma Aldrich, ~12600 g/mol). Both solutions were stirred overnight before being combined. Then, 1.1028g of Cu $(NO_3)_2$•$2.5H_2O$ was added to achieve the desired copper loading of 8 wt. % in the final Cu-SiO_2 material. The formulation was varied by changing the molar amount of MPTMS added, in order to reach a "Cu: MPTMS" molar ratio of either 1:0, 2:1, 1:1, or 1:2. The TEOS dosage was adjusted accordingly to maintain a constant Si content. The resulting homogeneous solution was then atomized using a TSI Incorporated® atomizer at an air pressure of 207 kPa. The aerosol was passed through a heated quartz tube in a tubular furnace set at 723 K to dry the droplets. The residence time of the droplets in the heated zone of the tube was in the order of ~1 second. The dried particles were collected on a nitrocellulose filter (Sartorius Stedim, 0.45 μm). The powders were then calcined in a muffle furnace under static air at 623 K for 3 hours (1 K/min), followed by an

increase to 823 K at a rate of 1 K/min for an additional 3 hours. The catalyst without MPTMS was labelled as Cu/Si while the catalysts made with MPTMS were labelled as Cu/SiM-(X), where X indicates the molar ratio between the number of moles of MPTMS and the number of moles of Cu.

A benchmark catalyst was prepared using a dry impregnation method with an aerosol made silica (support). This support was generated using the same procedure as for the Cu/Si catalyst but without the incorporation of copper nitrate. For impregnation, copper was introduced into the preformed silica by wetting it with an aqueous solution of $Cu(NO_3)_2$-$2.5H_2O$ (Alfa Aesar, 98% by weight) added dropwise using a syringe. The volume of solution used was calculated to correspond to the pore volume of the silica support, as evaluated by N_2 physisorption. After impregnation, the powders were subjected to calcination in a muffle furnace under static air conditions at 823 K for 3 hours, with a ramp rate of 1 K/min. The resulting catalyst was designated as I-Cu/Si, where "I" stands for "impregnation".

2.2 Characterization techniques

Details of the characterization analyses (N_2 physisorption, ICP-AES, XRD, XPS, electron microscopy, dispersion measurements, TPR, TPD, Uv-VIS) are provided in the ESI.

2.3 Catalytic test

The catalytic tests were carried out in a fixed-bed reactor (stainless steel, 0.6 cm internal diameter, 28 cm long) housed in a furnace (Minicor 42 Coreci) with internal thermocouple near the catalytic bed. 50 mg of calcined catalysts (sieved in the 0.20-0.40 mm range) were diluted with glass beads (0.5-1.0 mm). Before the reaction, the catalysts underwent in situ pre-reduction by hydrogen feed (21% H_2 in N_2, total flow rate 175 ml/min) for 30 minutes at 573 K with a ramp-up rate of 7 K/min, except for the benchmark sample for which pre-reduction was carried out at 623 K with a ramp-up rate of 7 K/min. The reactor was then adjusted to the desired reaction start temperature of 423 K.

Absolute ethanol was introduced via an NE-300 syringe pump into a stream of N_2, to obtain the desired mole fraction in the gas phase (1.6 mol%, total flow rate 110 ml/min). WHSV: $4h^{-1}$. All measurements were carried out at atmospheric pressure with temperatures gradually increased from 423 K to 673 K, maintaining each temperature for 1 hour to ensure stable conditions. In a variation of the test, the step-mode temperature increase was performed until 623 K and then this temperature was maintained for 16 hours. Standard stability tests were also carried on Cu/Si

and Cu/SiM1 by maintaining them directly at a reaction temperature of 573 K or 623 K for 24 hours.

The off-gases were analysed online using a VARIAN 3800 gas chromatograph equipped with a flame ionisation detector (FID) set at 463 K and a Restek Rt-U-BOND column (30 m long, 0.32 mm internal diameter, 10 μm film thickness). The GC programme was started at 383 K for 6 minutes, increased to 423 K at a rate of 10 K/min and stopped for 4 minutes. 1 min is needed to cool down. Four injections were carried out at each temperature and averaged. Carbon balance was found to close at 100 ±6 %. Ethanol and all the possible products were separately identified using pure standards and quantified via external calibration method.

Ethanol conversion (X_{EtOH}) was calculated as follows:

$X_{EtOH} = n_{EtOH(in)} - n_{EtOH(out)} / n_{EtOH(in)}$

Selectivity (Si):

$S_i = \nu_i n_i / (n_{EtOH(in)} - n_{EtOH(out)})$

In this formula, ν_i is the ratio of stoichiometric reaction coefficients, n_i denotes the molar flow of the product i, $n_{EtOH(in)}$ and $n_{EtOH(out)}$, represent the molar flows of ethanol entering and exiting the reactor, respectively.

Deactivation was evaluated using the integrated form of a first-order type deactivation model, and thus calculating the deactivation constant k_d

$$k_d = \frac{\ln\left(\frac{1 - Final\ Conversion}{Final\ Conversion}\right) - \ln\left(\frac{1 - Initial\ Conversion}{Initial\ Conversion}\right)}{t}$$

Where t is the reaction time-on-stream at a determined temperature, *Initial Conversion* and *Final Conversion* are the ethanol conversion at the beginning and the end, respectively.

3. RESULTS AND DISCUSSION

The actual copper content was determined by ICP analysis (Table S1), which showed values close to the nominal (theoretical) loadings, thereby confirming the reliability of the synthesis procedure.

All calcined catalysts exhibited a mesoporous structure, as evidenced by type IV nitrogen adsorption–desorption isotherms with a characteristic H2 hysteresis loop (Fig. S1, A). The

asymmetry of the hysteresis - with a steeper desorption branch relative to the adsorption branch - is indicative of pore constrictions (bottlenecks) within the mesoporous network. Pore size distribution (Fig. S1B) was centered between 7 and 10 nm. The forced closure of the hysteresis loop at relative pressures (p/p_0) between 0.4 and 0.5 suggests the presence of mesopores smaller than approximately 4 nm. The average pore volumes ranged from 0.49 $cm^3 \cdot g^{-1}$ for the bare (aerosol made) silica to 0.43–0.45 $cm^3 \cdot g^{-1}$ for the copper-containing catalysts, irrespective of the amount of sulfur introduced during synthesis. Similarly, no significant variation was observed in the specific surface area (SSA), which ranged between 350 and 430 $m^2 \cdot g^{-1}$ for all samples, except I-Cu/Si (300 $m^2 \cdot g^{-1}$) probably owing to the partial filling of the silica pores during impregnation. This consistency in textural properties, irrespective of the addition of MPTMS, suggests that this additive did not interfere with the pore formation process.

Diffraction patterns of the bare support (Fig. 1) showed a broad band around 2θ = 20-30°, corresponding to the amorphous nature of silica. Diffraction patterns of benchmark I-Cu/Si clearly showed CuO intense and sharp peaks in the 2θ range 35-80° indicating a high degree of crystallinity. Average crystallite size (estimated via the Scherrer equation on the 35.59° and 38.76° peaks) was evaluated to be 30 nm. For Cu/Si (prepared in one step, in the absence of MPTMS) two features at $2\theta \approx 35.59°$ and 38.76° were detected indicating the presence of small copper oxide nanoparticles (vide infra for TEM and dispersion experiments). However, with the addition of MPTMS, these XRD reflection lines gradually diminished (Cu/SiM0.5) and then fully disappeared (Cu/SiM1 and Cu/SiM2). This result indicates that the incorporation of the thiolated precursor during synthesis significantly affected the spatial distribution of the active phase, i.e. it favored Cu oxide dispersion.

The impact of MPTMS on Copper based nanoparticles was further corroborated by the UV-Vis spectra of Cu/SiM0.5, Cu/SiM1 and Cu/SiM2 (Fig. S2) which showed, with respect to Cu/Si, a noticeable blue shift, implying a modification in the electronic environment of Cu^{2+} ions. This can indicate a decrease in Cu particle size or/and to a better insertion of Cu ions within the SiO_2 matrix.

TEM and HAADF-EDX imaging provided clear evidence of the effect of MPTMS addition (Fig. 2). In the case of Cu/Si, although larger aggregates outside of silica spheres were also detected in rare spots (ESI Fig. S3), the metal species were mostly well dispersed (Fig. 2A-D), with particle size distribution centered around 2 nm (Fig. S4 A). In contrast, when MPTMS was used as an additive in the preparation, the sample exhibited a homogeneous copper dispersion

across all analyzed silica spheres (e.g. Cu/SiM1, Fig. 2E–H), with particles size distribution centered near 2 nm (Fig. S4 B).

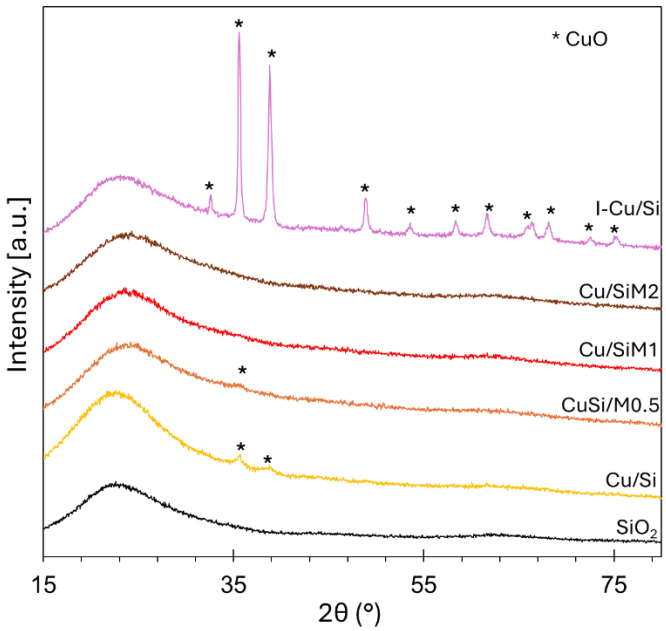

Figure 1: XRD patterns of the prepared catalysts after calcination.

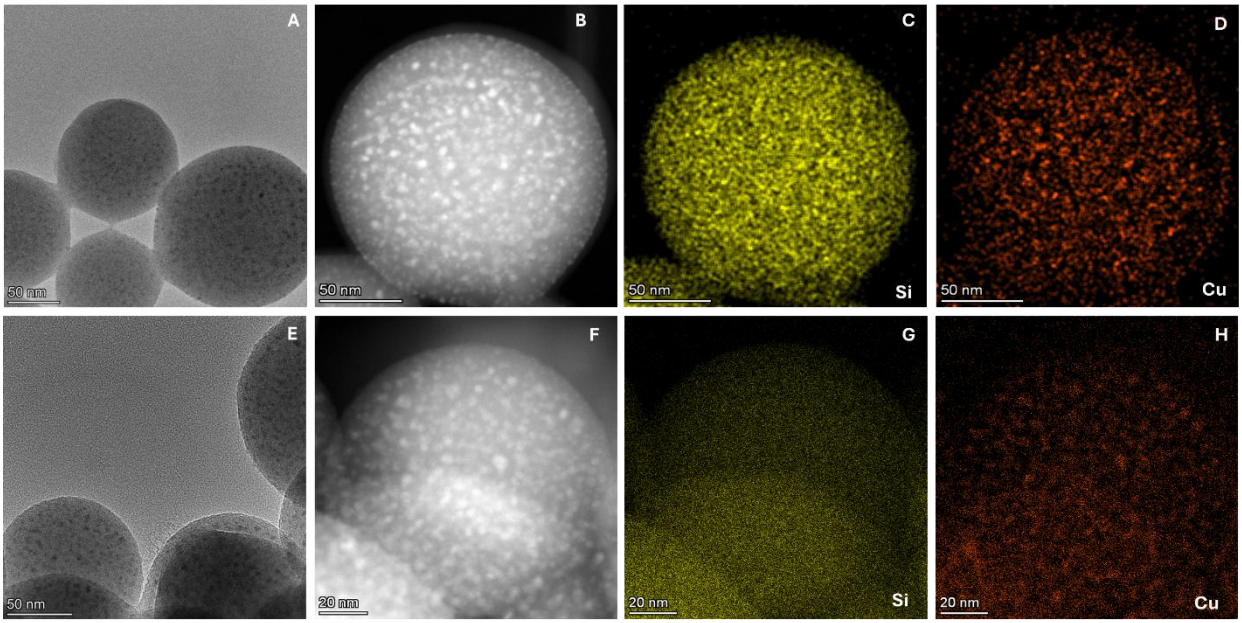

Figure 2: TEM (A) and HAADF-EDX (B-D) images of Cu/Si; TEM (E) and HAADF EDX (F-H) images of Cu/SiM1

The influence of MPTMS addition on both particle size and reducibility was further elucidated by H_2-TPR measurements (Fig. 3A). Reduction peaks fit well with the fact that all the Cu (as measured by ICP and compared in table S1) is present in the form of CuO and fully reduced to Cu during TPR. It also indicates that all the Cu, in all samples is indeed accessible to reduction. In I-Cu/Si, the reduction profile displays a clear bimodal particle-size distribution, with the dominant contribution arising from large CuO particles, as reflected by the major reduction peak at 601 K. Instead, in Cu/Si, high-temperature reduction features centered at 600 K and 750 K remain visible, consistent with the presence of larger CuO particles or CuOx species more strongly embedded in the silica matrix. [16,29,30] In contrast, as MPTMS is introduced and its amount increased (from Cu/SiM0.5 to Cu/SiM2), these high-temperature features progressively diminish. This gradual suppression indicates a continuous shift from the original bimodal distribution toward a more monomodal one. In Cu/SiM1 and Cu/SiM2, this evolution culminates in a single, well-defined reduction peak at 540–550 K, signifying a narrow and uniform particle-size distribution.

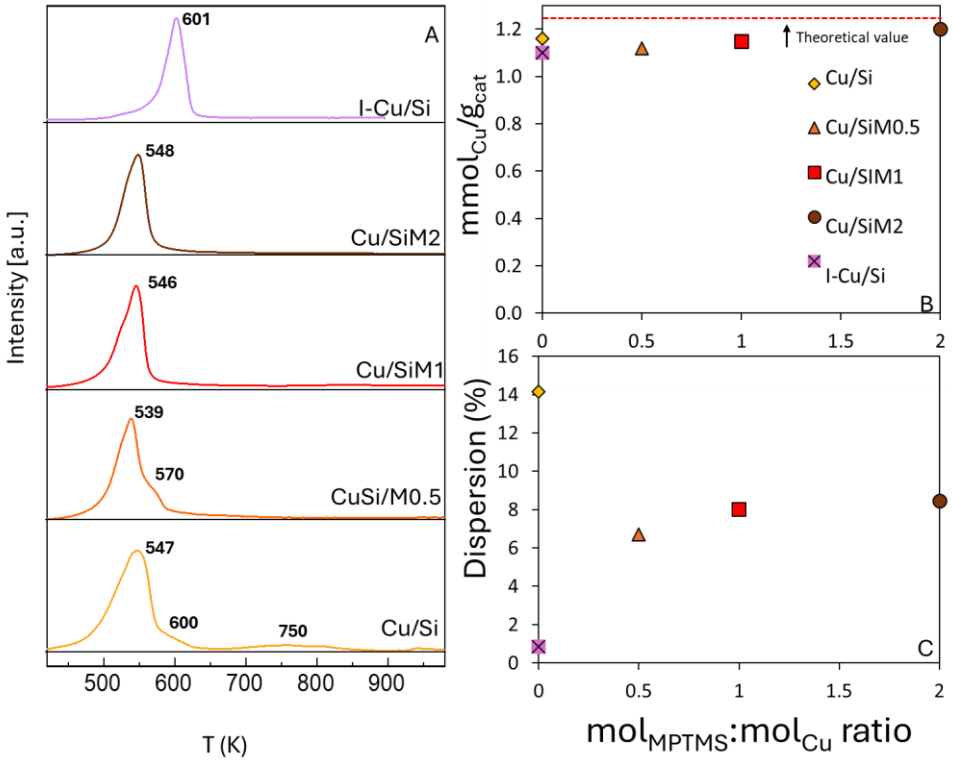

Figure 3: (A) TPR of calcined catalysts, (B) relative quantification of copper (from CuO via TPR experiment) and (C) dispersion measurements (via a sequential TPR-N_2O-TPR analysis).

Observing the dispersion values (Fig. 3, C), I-Cu/Si presented the lowest value (1%), which corroborates the formation of large CuO crystals and aligns with the XRD and TPR profile results. Contrarily, Cu/Si shows the highest dispersion (15%), indicating a greater amount of copper available on the surface in the form of small nanoparticles. In comparison, the MPTMS-containing catalysts showed lower dispersions (7-8%, almost not influenced the amount of MPTMS). This is in apparent contradiction with respect to the data gained from other characterization techniques, which indicated a finer dispersion of CuO when the aerosol preparation is done in the presence of MPTPS. It suggests that these smaller copper oxide particles were partially embedded into the silica matrix in the presence of MPTMS. Despite being smaller, their contribution to the "dispersion" parameter – defined as (Cu_{surf} / Cu_{tot}) – is lower.

The effect of MPTMS addition on the surface distribution of copper was also evaluated by XPS, both on non-calcined (NC) – i.e., directly after EISA (ESI Fig. S5 A, B) – and calcined samples (Fig. 4 A-C). In both cases, the high-resolution Cu 2p region revealed a main component centered at 933–934 eV, which can be attributed Cu^{2+} of bulk CuO,[31] but may also include contributions from Cu^{+} ions (i.e. assignable to Cu_2O) due to the relatively weak shake-up satellite at ~943 eV (typically ~50% in surface of the main peak for Cu^{2+}). A feature at 936 eV was also observed, which can be ascribed to highly dispersed Cu^{2+} ions in the silica matrix.[32]

In NC samples, sulfur was absent in the Cu/Si sample (Fig. 4D), and its surface content expectedly increased proportionally with the nominal S content (Fig. 4G). It appeared as R–SH with the characteristic doublet at ~163–164 eV [33,34], and as oxidized sulfur species (RSO_x: sulfoxides and/or sulfones) at ~166–170 eV [33]. This indicates that partial oxidation of the MPTMS thiol group likely occurred already during the AASG process (at 723 K under air). After calcination, S surface concentration dropped (the S/Si atomic ratio decreases from 0.04 to 0.01 for Cu/SiM1 and from 0.08 to 0.01 for Cu/SiM2), and a residual signal from oxidized sulfur remained detectable (ESI, Fig. S5 C, D).

Interestingly, with MPTMS addition, two main effects were observed over the calcined catalysts:

(i) a decrease in the overall Cu/Si surface ratio (Fig. 4H) corroborating the hypothesis that CuO nanoparticles are partially inserted in silica,

(ii) an increase in the Cu_{933}/Cu_{tot} ratio (Fig. 4I), suggesting a drop of inserted and dispersed Cu^{2+} ions with respect to CuO or Cu_2O particles.

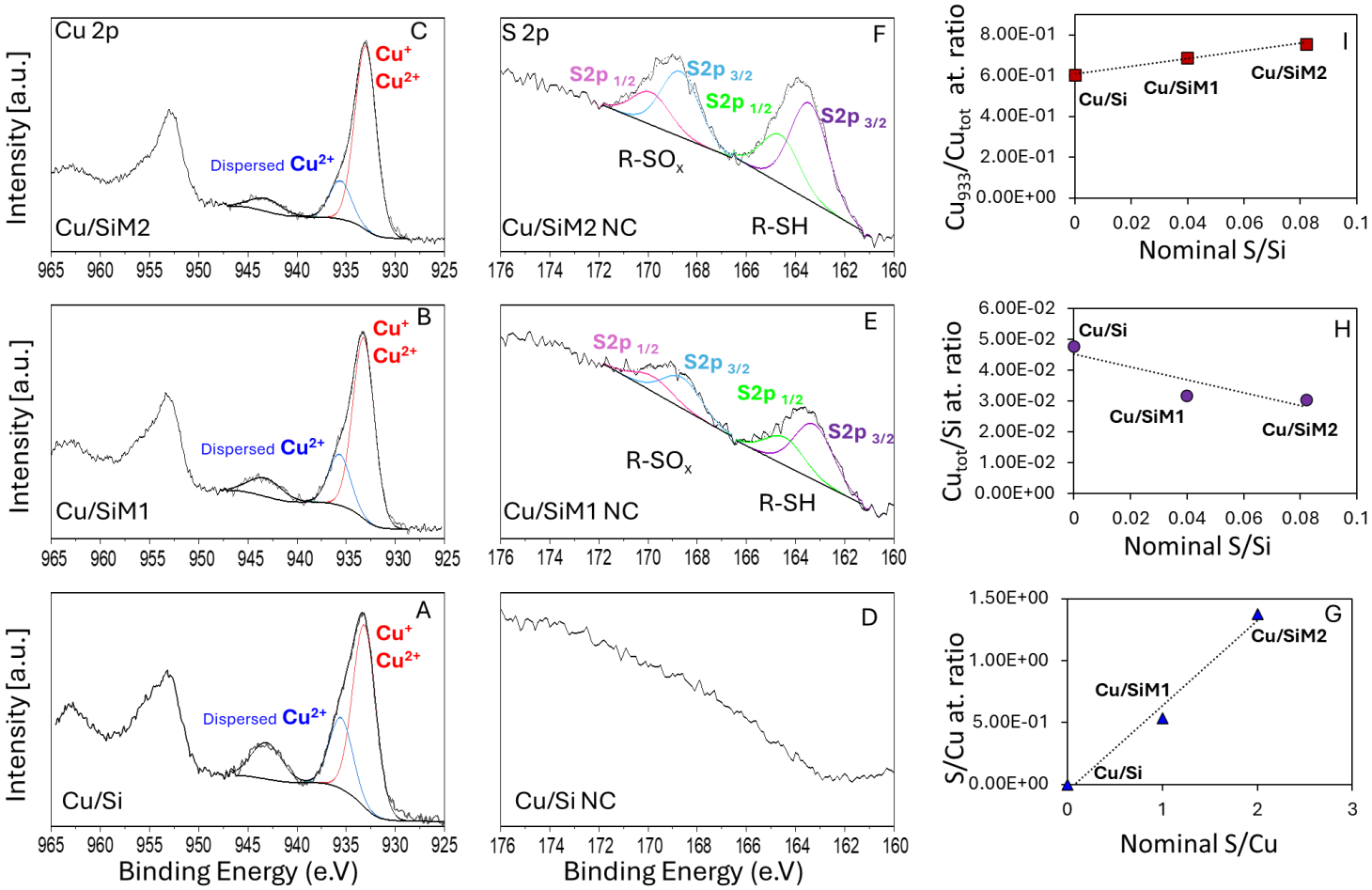

Figure 4: High resolution spectra of Cu 2p region for calcined samples (A, B, C) and of S 2p region for not calcined samples (D, E , F). Panel G shows the evolution of the S/Cu atomic ratio on not calcined samples as a function of the nominal S/Cu ratio. Panels H and I show the evolution of the Cu/Si and Cu_{933}/Cu_{tot} atomic ratios on calcined samples, as a function of the nominal S/Si atomic ratio.

Figure 5 A presents the ethanol conversion as a function of reaction temperature (423K-673 K) for the various catalysts tested (selectivity in Table S2). I-Cu/Si consistently exhibited low catalytic activity across the entire temperature range, with negligible conversion at 423 K and a maximum of only 32% at 673 K. In contrast, Cu/Si showed significantly higher activity, achieving approximately 90% ethanol conversion at 573 K. At the same temperature, catalysts synthesized with MPTMS showed notably lower conversion: 34% for Cu/SiM0.5, 44% for Cu/SiM1, and 30% for A- for Cu/SiM2, indicating that Cu/Si catalyst was initially more active.

However, a distinct shift in performance was observed above 573 K. While conversion decreased markedly for Cu/Si – dropping to 62% at 673 K – the MPTMS-modified catalysts displayed a progressive increase in conversion, ultimately surpassing 95% at the highest temperature (673 K). Selectivity remained similar or slightly higher for the catalysts prepared in the presence of MPTMS (Table S2). Among these, Cu/SiM1 exhibited the highest ethanol conversion, particularly at 623 K and 673 K, outperforming all the other catalysts. This inversion in catalytic performance suggests that the MPTMS addition affected the resistance of copper species against deactivation, likely by mitigating sintering and/or coking phenomena that severely impact Cu/Si at elevated temperatures.

Stability tests at 573 K (Fig. 5 B) and 623 K (Fig. 5 C) clearly confirmed the superiority of Cu/SiM1 with respect to Cu/Si upon 24h time on stream. In both cases, almost full selectivity to acetaldehyde was maintained (Tables S3 and S4). At 573 K, deactivation (here defined via the deactivation constant k_d) was 0.11 h^{-1} for Cu/Si but only 0.02 h^{-1} for Cu/SiM1. At 623 K, where sintering often rapidly occurs in Cu based catalysts [12], the difference was still evident, with a k_d of 0.08 h^{-1} for Cu/Si and only 0.03 h^{-1} for Cu/SiM1. All in all, combing ramping test and stability test (Fig. 5 D, see experimental section for details) further highlighted the better stability of Cu/SiM1 as compared to Cu/Si, showing a k_d of only 0.04 h^{-1} and 0.13 h^{-1} respectively (selectivity remained similar for both catalysts, above 90%, Table S5).

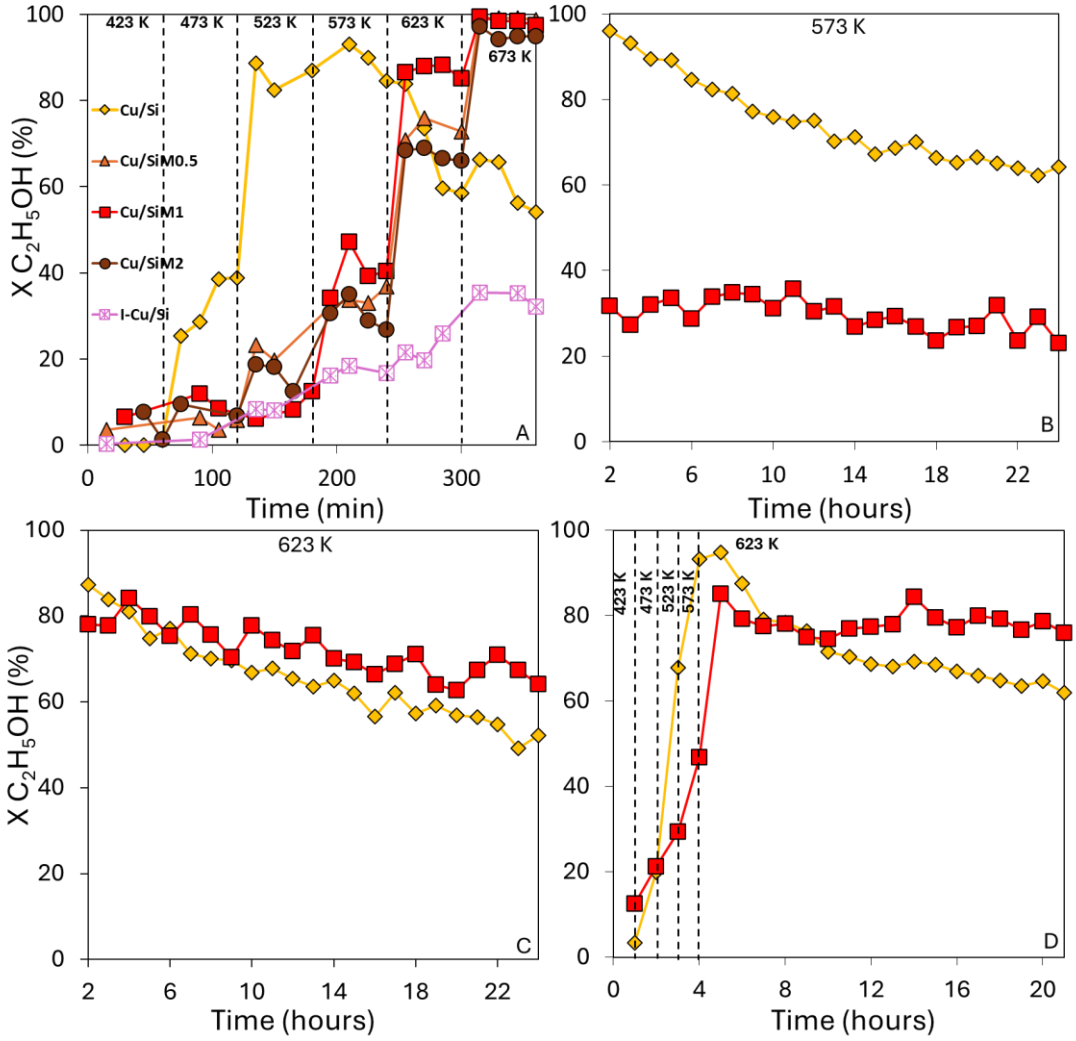

Figure 5: catalytic test between 423 K and 673 K (A), 24 h stability tests at 573 K (B) and at 623 K (C), catalytic test with combination of ramping and stability at 623 K (D).

XRD analysis of the spent catalysts (Fig. 6) confirmed the presence of metallic Cu as the dominant crystalline phase. This was particularly evident for I-Cu/Si, which exhibited sharp and intense diffraction peaks, indicative of pronounced sintering (Fig. 6 A). Crystal size was evaluated to be ≃47 nm. In contrast, for Cu/Si and samples Cu/SiM$_x$, only a weak reflection at 2θ = 43.3° – corresponding to the (111) plane of metallic Cu – was discernible. After 24 hours on stream at 573 K and 623 K (Fig. 6 B, C), characteristic reflections of metallic Cu at 2θ = 43.3° and 50.4° ((111) and (200) planes, respectively) were observed in both Cu/Si and Cu/SiM1. However, these peaks were significantly less intense in Cu/SiM1, suggesting a lower degree of copper sintering. At 623 K, a confirmation arose also from crystal size evaluation which resulted in ≃45 nm for Cu/Si and ≃25 nm for Cu/SiM1.

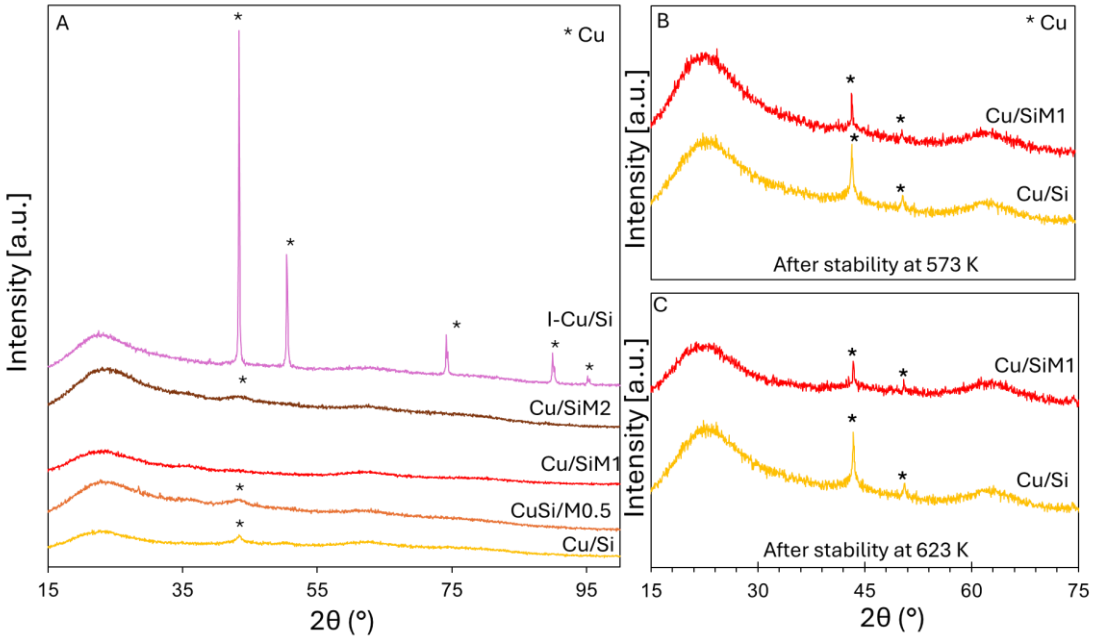

Figure 6: XRD analysis of spent catalysts after ramping test (A) and stability tests at 573 K (B) and at 623 K (C).

Looking at TEM microphotographs of spent Cu/Si (Fig. 7 A-C), well dispersed copper species were detected, together with larger aggregates at the surface of the microspheres (up to 100 nm). Particle size distribution was indeed broader with a mean focused at 42 nm (Fig. S6 A). Instead, in the case of spent Cu/SiM1 (Fig. 7 D-G), only dispersed copper species were observed (homogeneous particle size around 2.2 nm, Fig. S6 B) and no signs of further copper migration/exsolution were revealed.

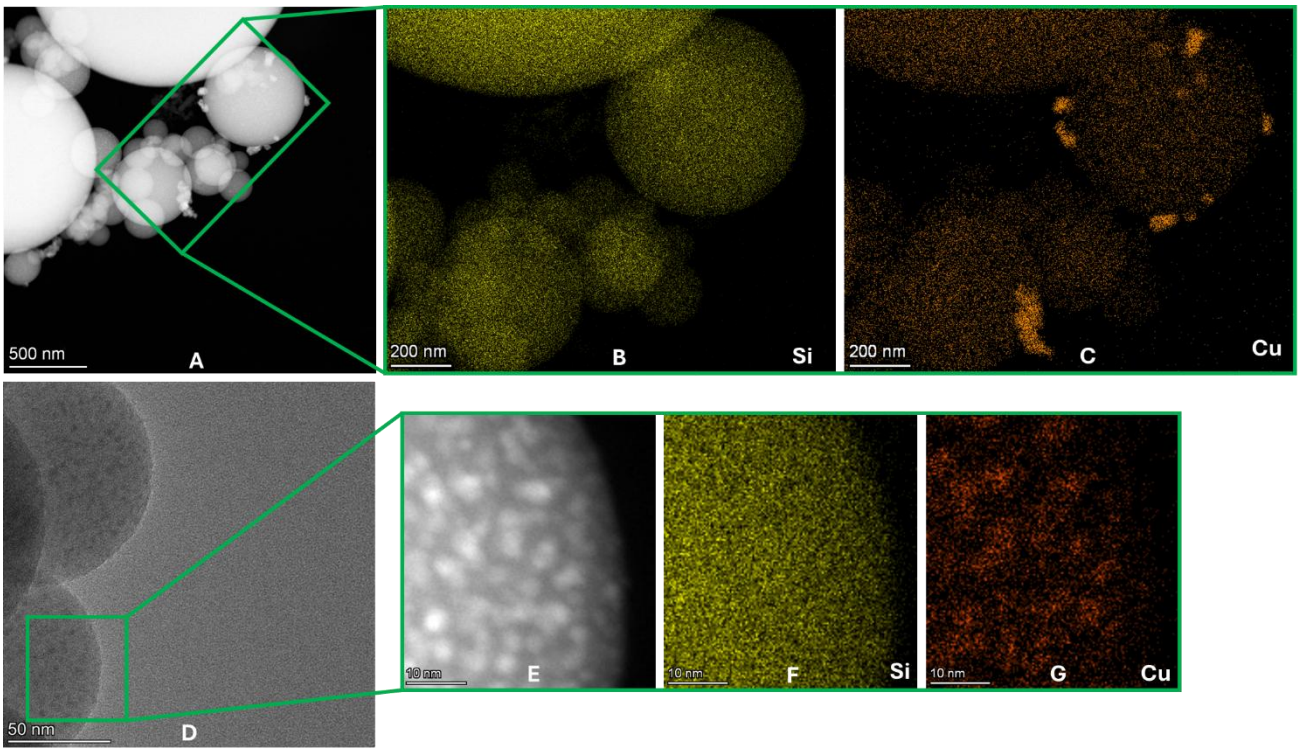

Figure 7: HAADF-EDX (A-C) images of spent Cu/Si; TEM (D) and HAADF EDX (E-G) images of spent Cu/SiM1

Surface analysis of spent catalysts by XPS (Fig. S7) corroborated the structural observations obtained from XRD and TEM. Specifically, Cu/Si exhibited a notable decrease in the Cu/Si atomic ratio following the catalytic reaction, indicative of metal sintering, whereas Cu/SiM1 preserved its initial surface composition, suggesting enhanced stability under reaction conditions.

Carbonaceous species were analyzed via the C 1s region (Fig. S7), which was deconvoluted into four main contributions: O–C=O, C=O/O–C–O, C–O, and C–(C,H). A general increase in carbonaceous deposits was observed post-reaction, consistent with carbon accumulation during catalysis. Importantly, while Cu/Si and I-Cu/Si showed only modest increases, Cu/SiM1 exhibited a markedly higher carbon accumulation – approximately fivefold greater. This pronounced carbon buildup on Cu/SiM1 correlates with its superior catalytic performance, suggesting that carbon deposition in this context is turnover-based but is not the main cause of catalyst deactivation. Moreover, as previously reported [35], dispersion of active phase is intrinsically correlated with acidity of copper based nanoparticles. Cu/SiM1, being more resistant to sintering and maintaining a higher dispersion (vide infra), possessed a higher acidity (Fig. S8).

The beneficial effect of MPTMS was also confirmed by dispersion measurements over spent catalysts (Fig. 8). Spent Cu/Si achieved a dispersion of 8% (compared with 14% on the fresh catalyst) highlighting a strong impact of reaction conditions on copper segregation. Conversely, Cu/SiM1 maintained a dispersion of 9% (consistent with the 8% before catalytic testing). Such results reinforce that the thiol group in MPTMS actively played a role in the structuring process of the catalysts, leading to a stabilization of the Cu species upon catalytic tests at high temperatures for prolonged time on stream.

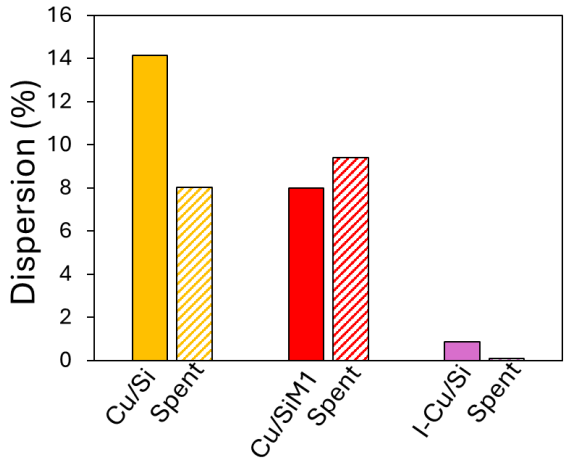

Figure 8: Dispersion values among fresh and spent catalysts (after ramping test).

4. CONCLUSIONS

Leveraging on the aerosol-assisted sol–gel process, mesoporous Cu–SiO_2 catalysts can be obtained in a one-pot and continuous manner. However, despite the improvement of such catalysts with respect to similar formulations prepared by classical impregnation, they still suffer from deactivation by sintering. Herein, we demonstrate that the in-situ stabilization of the copper precursor during synthesis using MPTMS suppresses the formation of large nanoparticles during aerosol processing and mitigates copper sintering during calcination under static air and during the catalytic tests, leading to small (2-4 nm), surface-accessible and stable copper nanoparticles homogeneously dispersed within the mesoporous silica support. In ethanol dehydrogenation, aerosol-made catalysts markedly outperformed the benchmark catalysts prepared by impregnation. At high reaction temperature (573-623 K), catalysts prepared in the presence of MPTMS exhibited markedly higher activity than the reference catalyst prepared in

the absence of MPTMS, while maintaining the same selectivity. Stability tests demonstrated that time-on-stream deactivation was strongly reduced in the MPTMS-promoted catalysts.

ACKNOWLEDGMENTS

This work was supported by the FNRS under Grant GEQ (Large Equipment) – UG01622F. Some of the results presented here were made possible thanks to infrastructure acquired under Measure BE-C[C72]-I[I-711], Research Platform for Energy Transition of the French Community of Belgium, funded through the REPowerEU chapter of the NextGenerationEU plan. G.P. thanks the Research Foundation Flanders (FWO Vlaanderen) for funding grant 1222525N.

REFERENCES

(1) Yuan, Q.; Wang, H.; Ding, W.; Zhu, Y. Biomass-Ethanol Conversion to Ethyl Acetate via One-Step Catalysis. *Green Chemical Engineering* **2025**.

(2) Dziugan, P.; Jastrzabek, K. G.; Binczarski, M.; Karski, S.; Witonska, I. A.; Kolesinska, B.; Kaminski, Z. J. Continuous Catalytic Coupling of Raw Bioethanol into Butanol and Higher Homologues. *Fuel* **2015**, *158*, 81–90.

(3) Zhang, M.; Yu, Y. Dehydration of Ethanol to Ethylene. *Ind. Eng. Chem. Res.* **2013**, *52* (28), 9505–9514.

(4) Yakovleva, I. S.; Banzaraktsaeva, S. P.; Ovchinnikova, E. V.; Chumachenko, V. A.; Isupova, L. A. Catalytic Dehydration of Bioethanol to Ethylene. *Catalysis in Industry 2016 8:2* **2016**, *8* (2), 152–167.

(5) Le Van Mao, R.; Nguyen, T. M.; McLaughlin, G. P. The Bioethanol-to-Ethylene (B.E.T.E.) Process. *Appl. Catal.* **1989**, *48* (2), 265–277.

(6) Phung, T. K. Copper-Based Catalysts for Ethanol Dehydrogenation and Dehydrogenative Coupling into Hydrogen, Acetaldehyde and Ethyl Acetate. *Int. J. Hydrogen Energy* **2022**, *47* (100), 42234–42249.

(7) Pampararo, G.; Debecker, D. P. Bioethanol as a Sustainable Platform Molecule for the Synthesis of Chemical Commodities. *Reference Module in Chemistry, Molecular Sciences and Chemical Engineering* **2025**, 304–323.

(8) Pang, J.; Yin, M.; Wu, P.; Li, X.; Li, H.; Zheng, M.; Zhang, T. Advances in Catalytic Dehydrogenation of Ethanol to Acetaldehyde. *Green Chemistry* **2021**, *23* (20), 7902–7916.

(9) Huang, Y.; Wang, B.; Yuan, H.; Sun, Y.; Yang, D.; Cui, X.; Shi, F. The Catalytic Dehydrogenation of Ethanol by Heterogeneous Catalysts. *Catal. Sci. Technol.* **2021**, *11* (5), 1652–1664.

(10) Patel, D. A.; Giannakakis, G.; Yan, G.; Ngan, H. T.; Yu, P.; Hannagan, R. T.; Kress, P. L.; Shan, J.; Deshlahra, P.; Sautet, P.; Sykes, E. C. H. Mechanistic Insights into Nonoxidative Ethanol Dehydrogenation on NiCu Single-Atom Alloys. *ACS Catal.* **2023**, *13* (7), 4290–4303.

(11) Franckaerts, J.; Froment, G. F. Kinetic Study of the Dehydrogenation of Ethanol. *Chem. Eng. Sci.* **1964**, *19* (10), 807–818.

(12) Pampararo, G.; Hlavenková, Z.; Styskalik, A.; Debecker, D. P. Suppressing On-Stream Deactivation of $CuSiO_2$ Catalysts in the Dehydrogenation of Bioethanol to Acetaldehyde. *Catal. Sci. Technol.* **2024**, *14* (17), 4912–4926.

(13) Pampararo, G.; Garbarino, G.; Riani, P.; Villa García, M.; Sánchez Escribano, V.; Busca, G. A Study of Ethanol Dehydrogenation to Acetaldehyde over Supported Copper Catalysts: Catalytic Activity, Deactivation and Regeneration. *Appl. Catal. A Gen.* **2020**, *602* (June), 117710.

(14) Vogt, E. T. C.; Fu, D.; Weckhuysen, B. M. Carbon Deposit Analysis in Catalyst Deactivation, Regeneration, and Rejuvenation. *Angewandte Chemie International Edition* **2023**, *62* (29), e202300319.

(15) Wintzheimer, S.; Luthardt, L.; Cao, K. L. A.; Imaz, I.; Maspoch, D.; Ogi, T.; Bück, A.; Debecker, D. P.; Faustini, M.; Mandel, K. Multifunctional, Hybrid Materials Design via Spray-Drying: Much More than Just Drying. *Advanced Materials* **2023**, *35* (47), 2306648.

(16) Pampararo, G.; Garbarino, G.; Riani, P.; Vykoukal, V.; Busca, G.; Debecker, D. P. Ethanol Dehydrogenation to Acetaldehyde with Mesoporous Cu-SiO_2 Catalysts Prepared by Aerosol-Assisted Sol–Gel. *Chemical Engineering Journal* **2023**, *465*, 142715.

(17) Pearson, R. G. Hard and Soft Acids and Bases, HSAB, Part 1: Fundamental Principles. *J. Chem. Educ.* **1968**, *45* (9), 581.

(18) Ophardt, C. E.; Wollaston, G. Redox Demonstrations and Descriptive Chemistry: Part 3. Copper (I)-Copper(II) Equilibria. *J. Chem. Educ.* **1991**, *68* (3), 248–249.

(19) Mautner, F. A.; Albering, J. H.; Harrelson, E. V.; Gallo, A. A.; Massoud, S. S. N-Bonding vs. S-Bonding in Thiocyanato-Copper(II) Complexes. *J. Mol. Struct.* **2011**, *1006* (1–3), 570–575.

(20) Ballarin, B.; Barreca, D.; Boanini, E.; Bonansegna, E.; Cassani, M. C.; Carraro, G.; Fazzini, S.; Mignani, A.; Nanni, D.; Pinelli, D. Functionalization of Silica through Thiol-Yne Radical Chemistry: A Catalytic System Based on Gold Nanoparticles Supported on Amino-Sulfide-Branched Silica. *RSC Adv.* **2016**, *6* (31), 25780–25788.

(21) Ballarin, B.; Barreca, D.; Boanini, E.; Cassani, M. C.; Dambruoso, P.; Massi, A.; Mignani, A.; Nanni, D.; Parise, C.; Zaghi, A. Supported Gold Nanoparticles for

Alcohols Oxidation in Continuous-Flow Heterogeneous Systems. *ACS Sustain. Chem. Eng.* **2017**, *5* (6), 4746–4756.

(22) Berezin, M. Y.; Wan, K. T.; Friedman, R. M.; Orth, R. G.; Raman, S. N.; Ho, S. V.; Ebner, J. R. Thiol Protected Platinum Black and Palladium Black Catalysts in Oxidation Catalysis. *J. Mol. Catal. A Chem.* **2000**, *158* (2), 567–576.

(23) Nichick, M. N.; Voitekhovich, S. V.; Lesnyak, V.; Matulis, V. E.; Zheldakova, R. A.; Lesnikovich, A. I.; Ivashkevich, O. A. 1-Substituted Tetrazole-5-Thiol-Capped Noble Metal Nanoparticles. *Journal of Physical Chemistry C* **2011**, *115* (34), 16928–16933.

(24) Wang, L.; Chen, M. X.; Yan, Q. Q.; Xu, S. L.; Chu, S. Q.; Chen, P.; Lin, Y.; Liang, H. W. A Sulfur-Tethering Synthesis Strategy toward High-Loading Atomically Dispersed Noble Metal Catalysts. *Sci. Adv.* **2019**, *5* (10).

(25) Van Der Verren, M.; Vykoukal, V.; Styskalik, A.; Malik, A. S.; Aprile, C.; Debecker, D. P. Airborne Preparation of Small Gold Nanoparticles Dispersed on Mesoporous Silica for the Catalytic Oxidation of Glycerol to Dihydroxyacetone. *ACS Appl. Nano Mater.* **2022**, *5* (12), 18977–18985.

(26) Pu, X.; Jiang, Z.; Hu, B.; Wang, H. γ-MPTMS Modified Nanometer-Sized Alumina Micro-Column Separation and Preconcentration of Trace Amounts of Hg, Cu, Au and Pd in Biological, Environmental and Geological Samples and Their Determination by Inductively Coupled Plasma Mass Spectrometry. *J. Anal. At. Spectrom.* **2004**, *19* (8), 984–989.

(27) Galehban, M. H.; Zeynizadeh, B.; Mousavi, H. Diverse and Efficient Catalytic Applications of New Cockscomb Flower-like Fe_3O_4@SiO_2@KCC-1@MPTMS@Cu II Mesoporous Nanocomposite in the Environmentally Benign Reduction and Reductive Acetylation of Nitroarenes and One-Pot Synthesis of Some Coumarin Compounds. *RSC Adv.* **2022**, *12* (18), 11164–11189.

(28) Zhan, G.; Zeng, H. C. Smart Nanocatalysts with Streamline Shapes. *ACS Cent. Sci.* **2017**, *3* (7), 794–799.

(29) Tkachenko, O. P.; Klementiev, K. V.; Van Den Berg, M. W. E.; Koc, N.; Bandyopadhyay, M.; Birkner, A.; Wöll, C.; Gies, H.; Grünert, W. Reduction of Copper in Porous Matrixes. Stepwise and Autocatalytic Reduction Routes. *Journal of Physical Chemistry B* **2005**, *109* (44), 20979–20988.

(30) Tohidi, S. H.; Gholamzadeh, S.; Shirazi, M. A. Z.; Novinrooz, A. J. Characterization of Sol–Gel Derived CuO/SiO_2 Nanostructure on Temperature. *International Journal of Industrial Chemistry 2014 5:3* **2014**, *5* (3), 63–68.

(31) Guerrero-Ruiz, A.; Rodríguez-Ramos, I.; Siri, G. J.; Fierro, J. L. G. Joint Use of XPS and Auger Techniques for the Identification of Chemical State of Copper in Spent Catalysts. *Surface and Interface Analysis* **1992**, *19* (1–12), 548–552.

(32) Gervasini, A.; Manzoli, M.; Martra, G.; Ponti, A.; Ravasio, N.; Sordelli, L.; Zaccheria, F. Dependence of Copper Species on the Nature of the Support for Dispersed CuO Catalysts. *Journal of Physical Chemistry B* **2006**, *110* (15), 7851–7861.

(33) *X-ray Photoelectron Spectroscopy (XPS) Reference Pages: Sulphur*. https://www.xpsfitting.com/2009/06/sulphur.html (accessed 2025-08-04).

(34) Castner, D. G.; Hinds, K.; Grainger, D. W. X-Ray Photoelectron Spectroscopy Sulfur 2p Study of Organic Thiol and Bisulfide Binding Interactions with Gold Surfaces. *Langmuir* **1996**, *12* (21), 5083–5086.

(35) Pampararo, G.; Scotti, N.; Zaccheria, F.; Ravasio, N.; Debecker, D. P. Dispersion-Driven Lewis Acidity of Cu–SiO_2 Catalysts. *Catal. Sci. Technol.* **2026**, *16* (2), 525–538.